Effect of Second-Order and Fully Nonlinear Wave Kinematics on a Tension-Leg-Platform Wind Turbine in Extreme Wave Conditions

Preprint

Antonio Pegalajar-Jurado, Michael Borg, and Henrik Bredmose
Technical University of Denmark

Amy Robertson and Jason Jonkman
National Renewable Energy Laboratory

Presented at the American Society for Mechanical Engineers' 36th International Conference on Ocean, Offshore & Arctic Engineering
Trondheim, Norway
June 25–30, 2017

NREL is a national laboratory of the U.S. Department of Energy
Office of Energy Efficiency & Renewable Energy
Operated by the Alliance for Sustainable Energy, LLC

This report is available at no cost from the National Renewable Energy Laboratory (NREL) at www.nrel.gov/publications.

Conference Paper
NREL/CP-5000-68049
August 2017

Contract No. DE-AC36-08GO28308

NOTICE

This report is available at no cost from the National Renewable Energy Laboratory (NREL) at www.nrel.gov/publications.

Available electronically at SciTech Connect http:/www.osti.gov/scitech

Available for a processing fee to U.S. Department of Energy and its contractors, in paper, from:

U.S. Department of Energy
Office of Scientific and Technical Information
P.O. Box 62
Oak Ridge, TN 37831-0062
OSTI http://www.osti.gov
Phone: 865.576.8401
Fax: 865.576.5728
Email: reports@osti.gov

Available for sale to the public, in paper, from:

U.S. Department of Commerce
National Technical Information Service
5301 Shawnee Road
Alexandria, VA 22312
NTIS http://www.ntis.gov
Phone: 800.553.6847 or 703.605.6000
Fax: 703.605.6900
Email: orders@ntis.gov

Cover Photos by Dennis Schroeder: (left to right) NREL 26173, NREL 18302, NREL 19758, NREL 29642, NREL 19795.

NREL prints on paper that contains recycled content.

Proceedings of the ASME 2017 International Conference on Ocean, Offshore and Arctic Engineering
OMAE 2017
June 25-30, 2017, Trondheim, Norway

OMAE2017-61798

EFFECT OF SECOND-ORDER AND FULLY NONLINEAR WAVE KINEMATICS ON A TENSION-LEG-PLATFORM WIND TURBINE IN EXTREME WAVE CONDITIONS

Antonio Pegalajar-Jurado
Technical University of Denmark
Department of Wind Energy
Kgs. Lyngby, DK-2800, Denmark
Email: ampj@dtu.dk

Michael Borg
Technical University of Denmark
Department of Wind Energy
Kgs. Lyngby, DK-2800, Denmark
Email: borg@dtu.dk

Amy Robertson
National Renewable Energy Laboratory
Golden, Colorado, 80401, USA
Email: amy.robertson@nrel.gov

Jason Jonkman
National Renewable Energy Laboratory
Golden, Colorado, 80401, USA
Email: jason.jonkman@nrel.gov

Henrik Bredmose
Technical University of Denmark
Department of Wind Energy
Kgs. Lyngby, DK-2800, Denmark
Email: hbre@dtu.dk

ABSTRACT

In this study, we assess the impact of different wave kinematics models on the dynamic response of a tension-leg-platform wind turbine. Aero-hydro-elastic simulations of the floating wind turbine are carried out employing linear, second-order, and fully nonlinear kinematics using the Morison equation for the hydrodynamic forcing. The wave kinematics are computed from either theoretical or measured signals of free-surface elevation. The numerical results from each model are compared to results from wave basin tests on a scaled prototype. The comparison shows that sub and superharmonic responses can be introduced by second-order and fully nonlinear wave kinematics. The response at the wave frequency range is better reproduced when kinematics are generated from the measured surface elevation. In the future, the numerical response may be further improved by replacing the global, constant damping coefficients in the model by a more detailed, customizable definition of the user-defined numerical damping.

Keywords: Numerical modeling; validation; aero-hydro-elastic code; floating wind turbine; nonlinear wave kinematics

INTRODUCTION

Floating wind turbines are becoming a realistic option for harvesting the vast offshore wind resources in deep water. The state-of-the-art numerical models for floating wind turbines often include linear or second-order modeling of the hydrodynamics. Nonlinear hydrodynamic effects can occur as a result of contributions from the wave kinematics, the hydrodynamic forcing, or both. Tension-leg platforms (TLPs) as substructures for floating wind turbines are stiffer in heave, roll, and pitch than other concepts, such as spar buoys or semisubmersibles. Hence, the natural frequencies in heave, roll, and pitch are higher for a TLP. Even though floating platforms are designed to avoid resonance with the range of wave forcing frequencies, resonance may still occur when sub or superharmonics of the incident waves resonate with one of the platform natural frequencies. Numerically, these harmonic components of the wave forcing are captured by models that include either nonlinear wave kinematics, nonlinear forcing, or both. The aim of this paper is to investigate the effect of nonlinear wave kinematics on the response of a TLP wind turbine by coupling an aero-hydro-elastic code with different wave kinematics models.

Within the numerical models used to compute wave loads in offshore applications, it is common to describe the incident wave kinematics with linear Airy theory [1] and the hydrodynamic forcing with either the slender-body Morison equation [2] or with potential-flow, radiation-diffraction solvers (e.g., output from the frequency-domain solver WAMIT [3] coupled to the time-domain dynamic model through the Cummins equation [4]). For irregular sea states, second-order wave kinematics can be obtained with, for example, Sharma and Dean's method [5]. Fully nonlinear kinematics, however, are rarely employed in the description of the wave field. Nonlinear models for the hydrodynamic forcing have been developed by Rainey [6, 7] and Sclavounos [8], although the Morison equation is also nonlinear in the drag term.

Nonlinear hydrodynamics specifically applied to a floating wind turbine have also been modeled with computational fluid dynamics (CFD) [9]. These models, although accurate, often do not include aerodynamics or wind turbine aeroelastic response, due to their higher computational cost. Hence, there is a need to couple nonlinear hydrodynamics with the current aero-hydro-elastic tools. The aeroelastic code FLEX5 [10] has already been coupled with fully nonlinear wave kinematics and Rainey forcing for studying the National Renewable Energy Laboratory's (NREL's) 5-MW reference wind turbine [11] mounted on a monopile [12–14]. The undisturbed, fully nonlinear wave kinematics were computed with OceanWave3D [15], a numerical tool developed at the Technical University of Denmark (DTU) able to perform large-scale, efficient, fully nonlinear and dispersive wave modeling for offshore engineering applications. The coupled FLEX5-OceanWave3D tool has also been employed to study the effects of nonlinear wave forcing on a TLP wind turbine [16, 17] by comparing the TLP response with different hydrodynamic models, but the results have not been compared to experimental data. A successful comparison of FLEX5 simulations on a TLP wind turbine to test data has been made by Pegalajar-Jurado et al. [18] within the LIFES50+ project [19], but only with undisturbed wave kinematics up to second order.

The aero-hydro-elastic code FAST [20], in its standard version [21], includes hydrodynamics based on either strip-theory Morison forcing or WAMIT output coupled with the Cummins equation. Second-order wave kinematics can be internally computed by FAST with the theory of Sharma and Dean [5] for the strip-theory solution. FAST has also been recently coupled with fluid-impulse theory (FIT) [22] and with second-order WAMIT output. Roald et al. [23] investigated the effect of WAMIT second-order forcing when FAST was not yet enabled to internally apply second-order WAMIT output. Hence, for their work, they linearized a FAST model of the floating wind turbine that included first-order WAMIT excitation forces and used the linearized model in WAMIT to compute the second-order response in the frequency domain. They followed this approach for a spar buoy and a TLP, and found that the effect of second-order forcing was more important for the TLP floater. However, the limitations of their work were those inherent to solving the equations of motion in the frequency domain (e.g., inability to capture transient effects or nonlinear mooring loads), as well as other limitations specific to WAMIT (e.g., wind turbine modeled as a rigid body, absence of aerodynamics and viscous drag). Later on, FAST incorporated the capability of taking WAMIT second-order output. This new capability was employed by Gueydon et al. [24] to investigate second-order hydrodynamic loads on a semisubmersible floating wind turbine. They found that, while superharmonic forces (namely sum-frequency loads, because they arise from the sum of any pair of frequencies in the first-order spectrum) seemed to have a negligible effect on the motions, subharmonic forces (or difference-frequency loads) were of considerable importance, introducing resonance with the surge natural frequency of the system, which is very low for this type of floater. The effect of second-order hydrodynamics on a TLP wind turbine was also investigated by Gueydon et al. [25] and Gueydon et al. [26], finding some influence of the superharmonic forcing on the pitch motion.

There is a need to investigate and compare to test data the effects of fully nonlinear hydrodynamics on a floating wind turbine within an aero-hydro-elastic model. In this paper, results from wave tank tests on a 1:60-scaled TLP wind turbine are used as a benchmark [27, 28]. These test results have already been used to validate a FLEX5 numerical model with Morison forcing, employing undisturbed linear and second-order wave kinematics (Pegalajar-Jurado et al. [29] and Pegalajar-Jurado et al. [18], respectively). For this work, the scaled floating wind turbine has been implemented in FAST and coupled with three different levels of wave kinematics: linear, second-order, and fully nonlinear representations of the undisturbed wave field. Under the assumption of a slender body, the hydrodynamic forcing is computed with the Morison equation. First- and second-order wave kinematics are externally computed in each case from a target, first-order, free-surface elevation. The fully nonlinear wave kinematics are extracted from OceanWave3D, in which the target free-surface elevation is imposed at the TLP location. A fourth case is also considered, in which the wave kinematics are computed directly from the measured surface elevation using first-order theory. The main reason to use the target free-surface elevation signal for three out of four models in this study is that, in most cases, designers do not have the corresponding experimental data and therefore they need to rely on theoretical environmental conditions for their computations. Thus, this paper does *not* present a validation study in the traditional sense, but instead, it can be seen as a "blind comparison," in which, for three out of four models, data for the actual environmental conditions in the tests are not available at the time of the numerical study. However, a subset

of the experimental data—namely free-decay tests and response to white noise waves—is still used to calibrate the models.

In this paper, the response of the TLP wind turbine is analyzed for extreme events represented by focused waves, as well as for irregular waves. The accuracy of the results with the different wave kinematics is assessed by comparing the predictions from each numerical model to the test data. Based on the comparison, the response phenomena and the accuracy of the forcing components of the waves are identified and discussed.

GENERAL APPROACH

For this work, results from laboratory tests on a 1:60-scaled TLP wind turbine are used as a benchmark for the numerical results obtained with a model of the same TLP wind turbine in the aero-hydro-elastic code FAST. The response of the TLP wind turbine to different extreme wave events is analyzed. The performance of the numerical model with different wave kinematics is assessed by comparing the numerical output to test data. A sketch of the approach followed in this study is shown in Fig. 1, which is explained in detail below. For each environmental condition, the starting point is the target, linear, free-surface elevation signal at the TLP location. During the test campaign, this target signal was converted into a control file and fed to the wavemaker in the test basin, where the TLP response was measured (black box labeled "Test response"). On the numerical side, the measured surface elevation at the TLP location was employed to compute linear wave kinematics, which were used as an input to FAST to produce a numerical response (dark yellow box labeled "FAST0 response"). The rest of the numerical responses stem from the target, linear, free-surface elevation, and correspond to the aforementioned concept of "blind comparison." The target signal was used as an input to obtain first- and second-order wave kinematics, which, once fed to FAST, resulted in the responses labeled FAST1 and FAST2 (blue and red boxes). It is relevant to state here that, for the FAST2 kinematics, the second-order terms were added to the target, first-order kinematics. Finally, the target signal was also employed as an input to generate fully nonlinear kinematics in OceanWave3D, corresponding to the response labeled as FAST3 (green box). All the five responses (Test, FAST0, FAST1, FAST2, and FAST3) to different environmental conditions are compared in the results section.

TEST DATA

The test campaign, extensively described in [27] and [28], was carried out in 2015 at DHI Denmark as part of the INNWIND.EU project [30]. The wave basin is 20 m long, 30 m wide and 3 m deep, which corresponds to a depth of 180 m in full scale. The TLP, which consists of a main floater, a transition piece, and four spokes (as shown in Fig. 2), was located 4 m

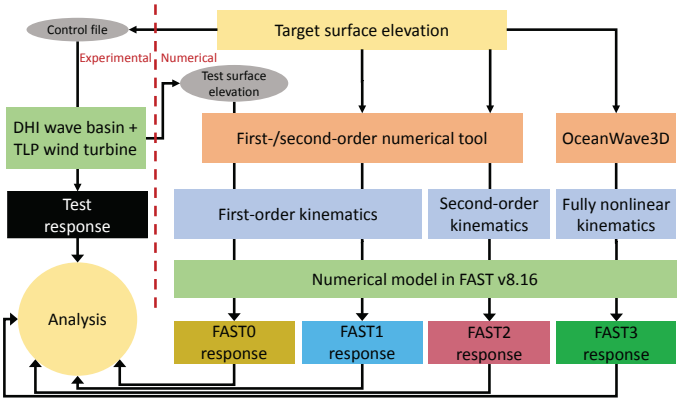

FIGURE 1. SKETCH OF THE GENERAL APPROACH. THE BOX COLOR FOR EACH OF THE FIVE RESPONSES IS CONSISTENT WITH THE PLOTS IN THE RESULTS AND DISCUSSION SECTION.

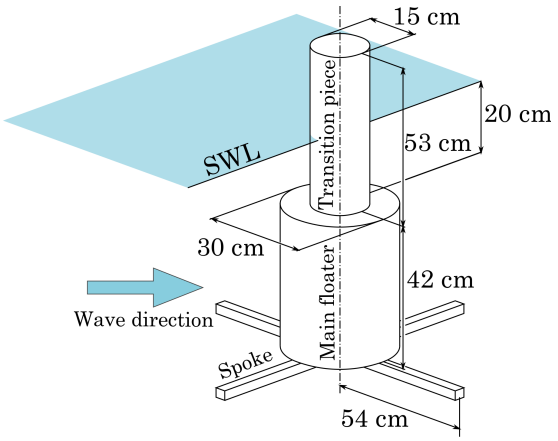

FIGURE 2. SKETCH AND DIMENSIONS OF THE SCALED TLP USED IN THE TESTS. SWL STANDS FOR STILL WATER LEVEL.

from the wave maker. Among others, the available test data includes wave elevation at several locations in the basin, nacelle acceleration, and floater motion in six degrees of freedom (surge, sway, heave, roll, pitch, and yaw) obtained with a Qualisys system. For this paper, attention will be given to free-surface elevation at the TLP location, floater surge and pitch, and nacelle acceleration. This data set has been previously used to validate a FLEX5 model of the same floating wind turbine [29] within the INNWIND.EU project, and it was found that the test pitch signal was amplified by a factor of 7.3 because of a calibration error. The same reduction factor 7.3 is applied to the test pitch signal for this study. A set of four environmental conditions has been chosen, namely two irregular and two focused waves, as seen in Tab. 1 below (the values are first given in lab scale and

TABLE 1. SELECTION OF TARGET ENVIRONMENTAL CONDITIONS.

Label	Type	Duration [s]	H_s or H_{max} [m]	T_p [s]
F3	Focused	30 (232)	0.102 (6.1)	-
F6	Focused	30 (232)	0.192 (11.5)	-
I3	Irregular	150 (1162)	0.055 (3.3)	0.84 (6.5)
I6	Irregular	150 (1162)	0.103 (6.2)	1.15 (8.9)

in parentheses in full scale). In the table, irregular sea states are defined by H_s and T_p—namely the target significant wave height and wave peak period, respectively—and were generated from a Pierson-Moskowitz spectrum. The focused waves, produced with linear New Wave theory [31] for the target wave spectrum, are defined by a linear target wave height of $H_{max} = 1.86H_s$, corresponding to the expected 3-hour Rayleigh-distributed wave height. For the irregular sea states, the first 60 seconds of transient response are removed from the analysis. All the sea states considered in this study are two dimensional (i.e., without spreading).

NUMERICAL MODEL

FAST [20], developed by NREL through U.S. Department of Energy support, is an open-source multiphysics tool practical to the engineering design of wind turbines, including both fixed-bottom and floating offshore wind turbines. FAST has the ability to input any externally generated wave kinematics and compute, in that case, the hydrodynamic forcing using the Morison equation. For this work, a FAST model of the 1:60 TLP wind turbine was developed. The model considers a rigid floating foundation and blades, whereas the tower is flexible and the mooring model is dynamic (the FAST MoorDyn module is used). No wind is considered in this paper, and the turbine is always in parked condition. The FAST model is combined with four different sets of wave kinematics, as detailed below.

Wave kinematics

For the selected environmental conditions, four versions of wave kinematics are given to FAST as an input, and the corresponding numerical responses are compared to test data. Figure 3 shows the free-surface elevation for environmental condition F6, including measured (test) free-surface elevation in the wave basin at the TLP location (with the floating structure present), first-order target signal, second-order signal, and free-surface elevation obtained from the OceanWave3D

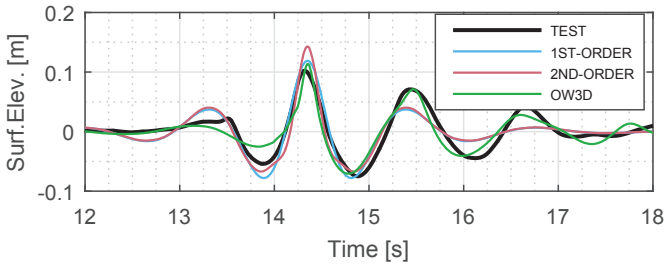

FIGURE 3. FREE-SURFACE ELEVATION SIGNALS FOR F6.

(OW3D) simulation. It is observed that the maximum peak in the second-order signal is larger than in the first-order signal. The maximum peak in the measured free-surface elevation is slightly below the target first-order peak. The OceanWave3D signal presents a good reproduction of the test signal both in the main peak and the one following. However, the peak to the left of the main peak (around 13.5 s) is not well captured by any of the numerical signals. Some details on the different wave kinematics used with the FAST model are given below:

- The label FAST1 corresponds to strictly linear wave kinematics computed from the target free-surface elevation signal (blue signal in Fig. 3). For consistency with linear Airy theory [1], the kinematics are computed up to still water level (SWL, $z = 0$).
- FAST2 corresponds to second-order wave kinematics computed from the target free-surface elevation signal using the theory of Sharma and Dean [5] (red signal in Fig. 3). The second-order terms are added to the first-order kinematics. This second-order solution is first computed up to SWL, and later truncated below (in the wave troughs) or extrapolated up to (in the wave crests) the surface elevation. Shown in Eqn. (1) is the extrapolation of the second-order horizontal particle velocity, $u^{(2)}$, for the region between SWL and first-order free-surface elevation, $0 < z <= \eta^{(1)}$:

$$u^{(2)}(x,z,t) = u^{(2)}(x,0,t) + z\frac{\partial u^{(1)}}{\partial z}\bigg|_{(x,0,t)} \quad (1)$$

  To keep the kinematics strictly second order, both the surface elevation and the slope employed in the extrapolation are first order.
- Fully nonlinear wave kinematics computed from the target surface elevation correspond to the label FAST3 (green signal in Fig. 3). The fully nonlinear kinematics, computed up to the free surface, are extracted from OceanWave3D [15]. In OceanWave3D, the input is the target, linear free-surface elevation at the desired location. For cases

where wave breaking occurs, OceanWave3D includes the option to enable an ad-hoc dissipation filter, which extracts energy from the system when the Lagrangian vertical particle acceleration $\dot{w}$ exceeds a certain limit, given by $-\dot{w} > \beta g$, where g is the gravitational acceleration and β is a user-defined parameter. The breaking filter, however, was not triggered in any of the cases for this study, which is consistent with the absence of wave breaking observed in the wave basin for these environmental conditions.

- The label FAST0 corresponds to linear wave kinematics computed from the measured surface elevation (black signal in Fig. 3). As it was done for FAST1, and to ensure consistency with linear wave theory, the FAST0 kinematics are also computed up to the SWL. However, although the test surface elevation is considered first order in this approach, it contains the nonlinearities developed in the wave basin tests.

All first- and second-order kinematics were computed with an external numerical tool, which has been validated against FAST internally computed wave kinematics. The maximum frequency considered in the Fourier analysis was 3.87 Hz (0.5 Hz in full scale) for FAST1 and FAST2 kinematics, because this was the cut-off frequency of the target surface elevation. On the other hand, kinematics for FAST0 were computed considering a maximum frequency of 7 Hz (0.9 Hz in full scale), given that the test surface elevation showed energy up to this frequency. The kinematics for FAST3 were taken as computed by OceanWave3D.

In cases where test data are available and a numerical reproduction of test results is sought, it is preferred to compute wave kinematics from the free-surface elevation measured at the wave basin (as in the cases labeled here with FAST0). However, although this approach is useful for resimulation of scaled tests and has previously provided good results [18, 29], it is not generally applicable for design—because it would require a laboratory test for each design case. From a designer's point of view, the use of the target signal as a starting point is more relevant. In this paper, we adopt both perspectives: one from a design point of view, where measured surface elevation is not available and therefore the target signal has to be employed in the computations (namely "blind comparison"), and one from a resimulation point of view, where the kinematics are computed from the test surface elevation.

Hydrodynamic forcing

A submerged body exposed to wave loads can be considered as slender—meaning that the effect of the body on the wave field is negligible, and therefore undisturbed wave kinematics can be used—when $D/L <= 0.2$, where D is the characteristic diameter of the body and L the characteristic wave length. For the environmental conditions considered in this study, L=1.3 m for F3 and L=1.8 m for F6. For the transition piece, D=0.15 m, therefore D/L=0.12 for F3 and 0.08 for F6. For the main floater D=0.3 m, therefore D/L=0.23 and 0.17 for F3 and F6, respectively. The spokes are considerably thinner than the floater or transition piece, therefore they are within the slender-body range of D/L. Although the main floater for the sea state F6 is outside the limit of the slenderness condition, the TLP was considered as slender for this study, and the hydrodynamic forcing was modeled using strip theory and the Morison equation [2]. The Morison inline force on a submerged body is given by

$$F_m = \int_{z_{body}} (0.5\rho C_D D(u-\dot{x})|u-\dot{x}| + \rho C_a A(u_t - \ddot{x}) + \rho A u_t) dz, \tag{2}$$

where ρ is the fluid density, D and A are the diameter and sectional area of the submerged body, and C_D and C_a are the drag and added-mass coefficient, respectively. The local particle velocity and Eulerian acceleration are u and u_t, whereas $\dot{x}$ and $\ddot{x}$ represent the body local velocity and acceleration, respectively.

Model calibration

During the test campaign, the natural frequencies of the scaled floating wind turbine were measured as 0.19 Hz for surge (0.025 Hz in full scale) and 1.9 Hz for the first coupled pitch-tower frequency (0.25 Hz in full scale). These natural frequencies were matched in the numerical model by calibration of a set of parameters. First, the natural frequency of the tower with clamped floater was matched by adjusting the tower stiffness. Next, the floater was released and the surge natural frequency was matched by adjusting the added-mass coefficients to $C_a = 0.77$ for the main floater and transition piece and $C_a = 1.2$ for the spokes. The heave natural frequency was matched by adjusting the axial vertical added-mass coefficient at the TLP bottom to $C_{a,ax} = 0.7$. The coupled pitch-tower natural frequency in moored condition was also matched by adjusting the floater mass moment of inertia. In the model, viscous hydrodynamic effects are introduced through the Morison drag forcing term and a linear damping matrix, constant both in space and frequency. The drag coefficients were first estimated based on Reynolds and Keulegan-Carpenter numbers and later tuned based on free-decay tests to $C_D = 0.6$ for the main floater, $C_D = 1$ for the transition piece, and $C_D = 1.2$ for the spokes. Further, the coefficients in the linear damping matrix were obtained by comparing the response of the FAST0 model to test data for a case with irregular waves from a white noise spectrum. These damping coefficients were also employed in FAST1, FAST2, and FAST3 versions of the model. After the linear damping coefficients were adjusted, it was observed that the numerical model could not reproduce exactly the surge and pitch decay tests. However, it was decided to keep the damping coefficients as calibrated against the white noise test, given that the response

to white noise provides information of the system in a broad range of frequencies, whereas decay tests contain information at only some frequencies—the system natural frequencies.

RESULTS AND DISCUSSION

In this section, the dynamic response of the TLP wind turbine to different environmental conditions is analyzed. Special attention is given to sub and superharmonic components in the response, which may excite the TLP surge natural frequency (at 0.19 Hz) and first coupled pitch-tower frequency (at 1.9 Hz). The ability of all models to correctly reproduce the response in the wave frequency range is also discussed. An analysis of extreme events for irregular waves, based on exceedance probability plots, is also included at the end of the section. Finally, some comments on the potential sources of uncertainty are made.

Response to focused waves

Results for the focused waves F3 and F6 are shown in Figs. 4 and 5, including time series and power spectral density (PSD) of free-surface elevation, platform surge and pitch, and nacelle acceleration. The PSD analysis is applied to the portion of time series shown in the time plot (i.e., between 12 and 18 s).

In surge, the test response for F3 is dominated by the surge natural frequency, whereas for F6 the test surge response at the wave frequency range is of similar magnitude. For both F3 and F6, the FAST1 model in surge only shows energy at the wave frequency range—as expected, given that the kinematics for that model are strictly linear and the loads are inertia-dominated, although some nonlinear effects may be introduced by the mooring lines. The surge response at the surge natural frequency for the FAST2 model matches the test signal for F3, but is largely overpredicted for F6. In the FAST3 model, the fully nonlinear kinematics introduce some subharmonic surge response as well, underpredicted for F3 but much closer to the tests for F6, as can be also observed in the surge time series for F6. The model FAST0 shows response at the surge frequency similar to FAST3, but it is the one to best reproduce the surge response at the wave frequency range. The rest of the models with kinematics from the target signal (FAST1, FAST2, FAST3) lack excitation at the wave frequency range, as could be anticipated from the differences in the wave spectra.

The pitch motion is dominated by the response at the wave frequency range, and FAST1, FAST2, and FAST3 models slightly overpredict the response at the coupled pitch-tower natural frequency (1.9 Hz) for F3, whereas FAST0 is the one closest to the test. For F6, the coupled pitch-tower frequency is not within the linear target wave spectrum, hence the FAST1 model shows no response. FAST0 is again the one to best predict the system pitch response at that frequency. The remaining two models—FAST2 and FAST3—overpredict the response at the pitch-tower frequency for F6, likely due to an excess of energy at this frequency in the superharmonic part of the wave spectrum. In nacelle acceleration, which is also dominated by the response at the wave frequency range, all models predict well the response at the pitch-tower frequency for F3 except for FAST0, which underpredicts it. For F6, FAST1 shows no response at the pitch-tower frequency and FAST3 overpredicts, whereas FAST0 and FAST2 are the ones to best reproduce the test response at the given frequency. In the wave frequency range, for both pitch and nacelle acceleration, the FAST0 model is again the best to reproduce the test response, although some overprediction is observed in pitch motion for F6.

It is observed that the response spectral differences at the wave frequency range between the FAST1, FAST2, and FAST3 models and the test are directly linked to the difference in wave spectrum. For F3, the wave spectra for FAST1, FAST2, and FAST3 are poorly reproduced, hence these models yield responses that poorly reproduce the test response at the wave frequency. For F6, the wave spectra are more similar, which is translated into a better match in the response at the wave frequency range for the three models. However, these discrepancies in model input—and, consequently, in model output—are inherent to the "blind comparison" approach employed for these three versions of the model.

Response to irregular waves

The response to irregular waves I3 and I6 is shown in the time and frequency domain in Figs. 6 and 7. The PSD analysis is applied to the entire time series after removal of transient (i.e., between 60 and 150 s). To improve readability, the PSD plots for irregular waves have been smoothed using local regression with weighted linear least squares, a first-degree polynomial model, and a span of 7 data points.

Frequency-wise, some of the observations already made for focused waves apply also for irregular waves. For I3, subharmonic surge response is largely overpredicted by FAST2, slightly underpredicted by FAST0, and well predicted by FAST1 and FAST3. The linear model FAST1, which did not show surge response at the surge frequency—where there is no linear wave energy—for focused waves, presents a certain amount of energy at this frequency for I3, likely due to nonlinear effects introduced by the mooring lines. For I6, FAST2 predicts well, FAST0 and FAST3 underpredict the surge response at the surge frequency, and FAST1 shows almost no response.

In the superharmonic region, FAST1 and FAST2 slightly overpredict the pitch motion at the pitch-tower coupled frequency for I3, whereas FAST0 and FAST3 underpredict it. The agreement is better for all models for I6. For nacelle acceleration, all four models largely underpredict the response at the coupled pitch-tower frequency for I3, whereas they all come

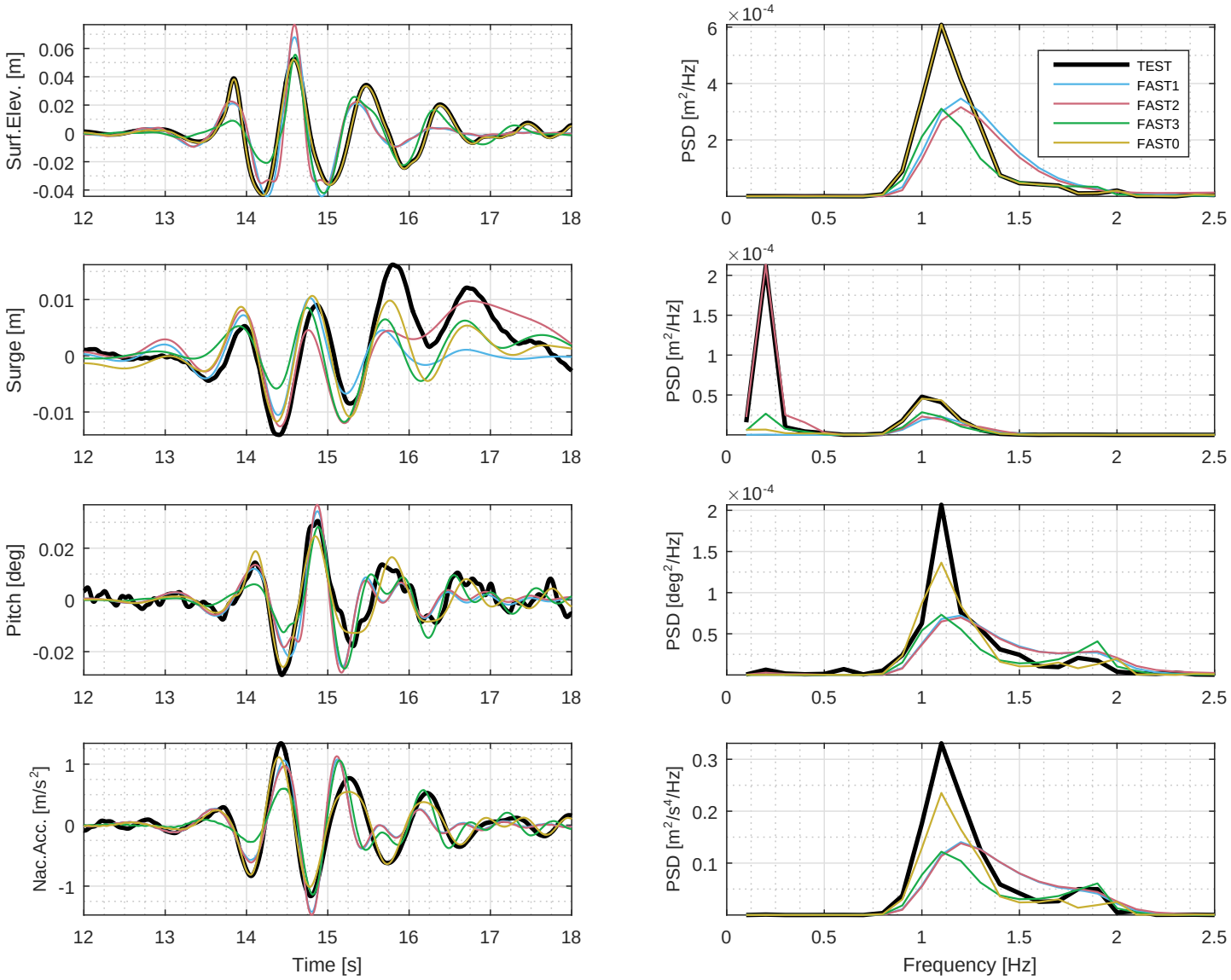

FIGURE 4. RESPONSE TO FOCUSED WAVE F3-TIME SERIES AND PSD.

much closer to the test response for I6—which is much lower than for I3, because of the differences in wave frequency ranges between I3 and I6.

A statistical analysis of the response for I3 and I6 was carried out through exceedance probability plots, which are presented in Figs. 8 and 9. The time series of free-surface elevation was divided into individual waves defined between zero-downcrossings, and a time window was defined for each individual wave. Within the given window, the peak of each response signal was stored. These peaks were then sorted and assigned an exceedance probability, P, based on their position in the sorted list. The results show that the measured free-surface elevation generally has higher peaks than its numerical versions, with the exception of the second-order signal for I6. In surge, FAST1 and FAST3 always underpredict the response, FAST0 is the closest one to the test (especially for I3), and FAST2 can be found on one side or the other depending on the sea state. In pitch, all models generally overpredict the response, with FAST3 being the one closer to the test in both sea states. Nacelle acceleration is overestimated by all models for I3, whereas they all provide a good prediction for I6.

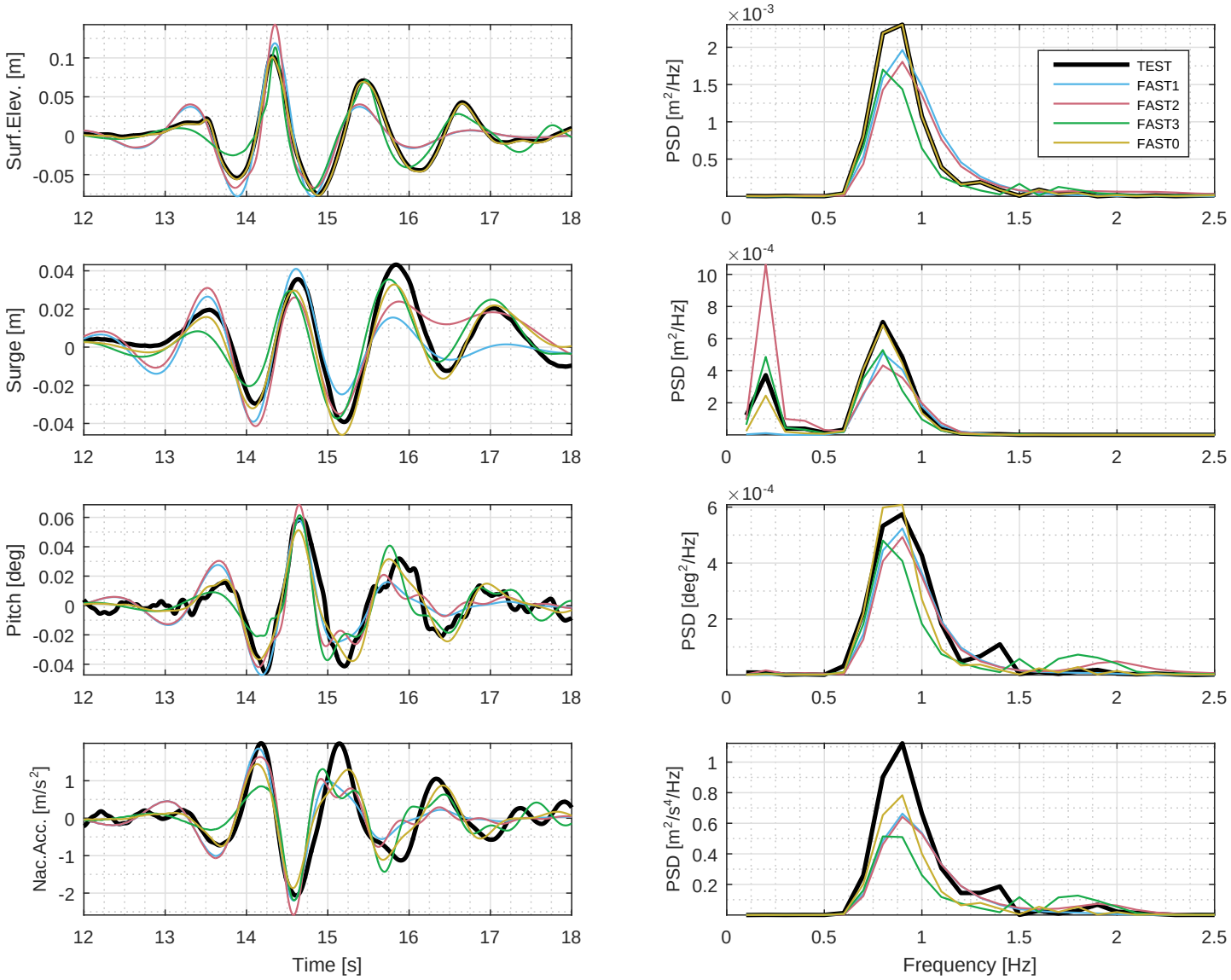

FIGURE 5. RESPONSE TO FOCUSED WAVE F6-TIME SERIES AND PSD.

Potential sources of uncertainty

There were some uncertainties associated with the wave basin tests that could lead to some discrepancies between test results and numerical predictions. These uncertainties include, among others, the measuring equipment, where the most notable uncertainty is associated to the aforementioned calibration error in the measured platform pitch signal, and the consequent reduction factor applied to it, as mentioned in the description of the test data.

Other sources of uncertainty are associated to the modeling approach. For three out of four models, the wave kinematics were purposedly computed from a free-surface elevation signal different to that measured in the test ("blind comparison" approach), which will introduce discrepancies. The hydrodynamic viscous effects were modeled through a linear damping matrix and a drag forcing term proportional to the square of the relative velocity. The drag coefficient was estimated and calibrated based on decay tests, whereas the damping coefficients were chosen based on a test with white noise waves. Structurally, some simplifications were also made in the numerical model. The connection between spokes and main floater was assumed to be rigid, but some flexibility was observed in the test prototype during the test campaign. The assumption of a rigid floating platform was made in this study because it is

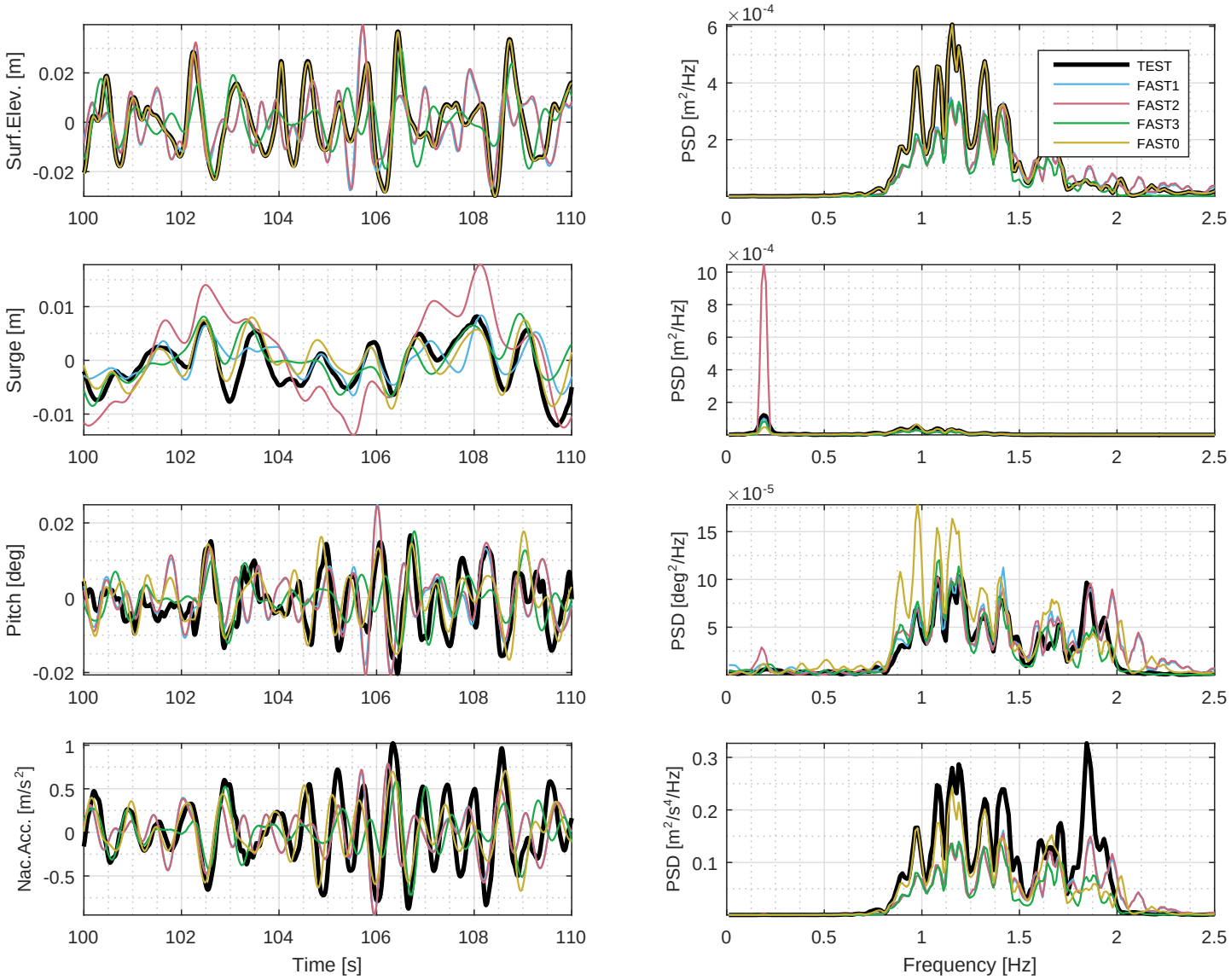

FIGURE 6. RESPONSE TO IRREGULAR WAVE I3-TIME SERIES AND PSD.

closer to the situation a designer is faced with. However, current trends in research that have included structural flexibility of the foundation in combination with radiation-diffraction potential flow hydrodynamic forcing [32] have found that there is an impact of floater flexibility on nacelle acceleration.

SUMMARY

The effect of linear, second-order, and fully nonlinear wave kinematics on the numerical response of a TLP wind turbine was analyzed and discussed. The choice of signal for free-surface elevation—from which wave kinematics are computed—has also been investigated.

The use of second-order and fully nonlinear wave kinematics introduces subharmonic forcing that, in some cases, brings the numeric response closer to the test benchmark. In the superharmonic region, when there is linear wave energy, all models are able to show response at the coupled pitch-tower natural frequency. When such linear wave energy is not present, second-order and fully nonlinear wave kinematics also introduce energy at the pitch-tower frequency.

By using the test free-surface elevation as the input to first-order wave kinematics, the system response at the wave frequency range is clearly improved. With this approach, some of

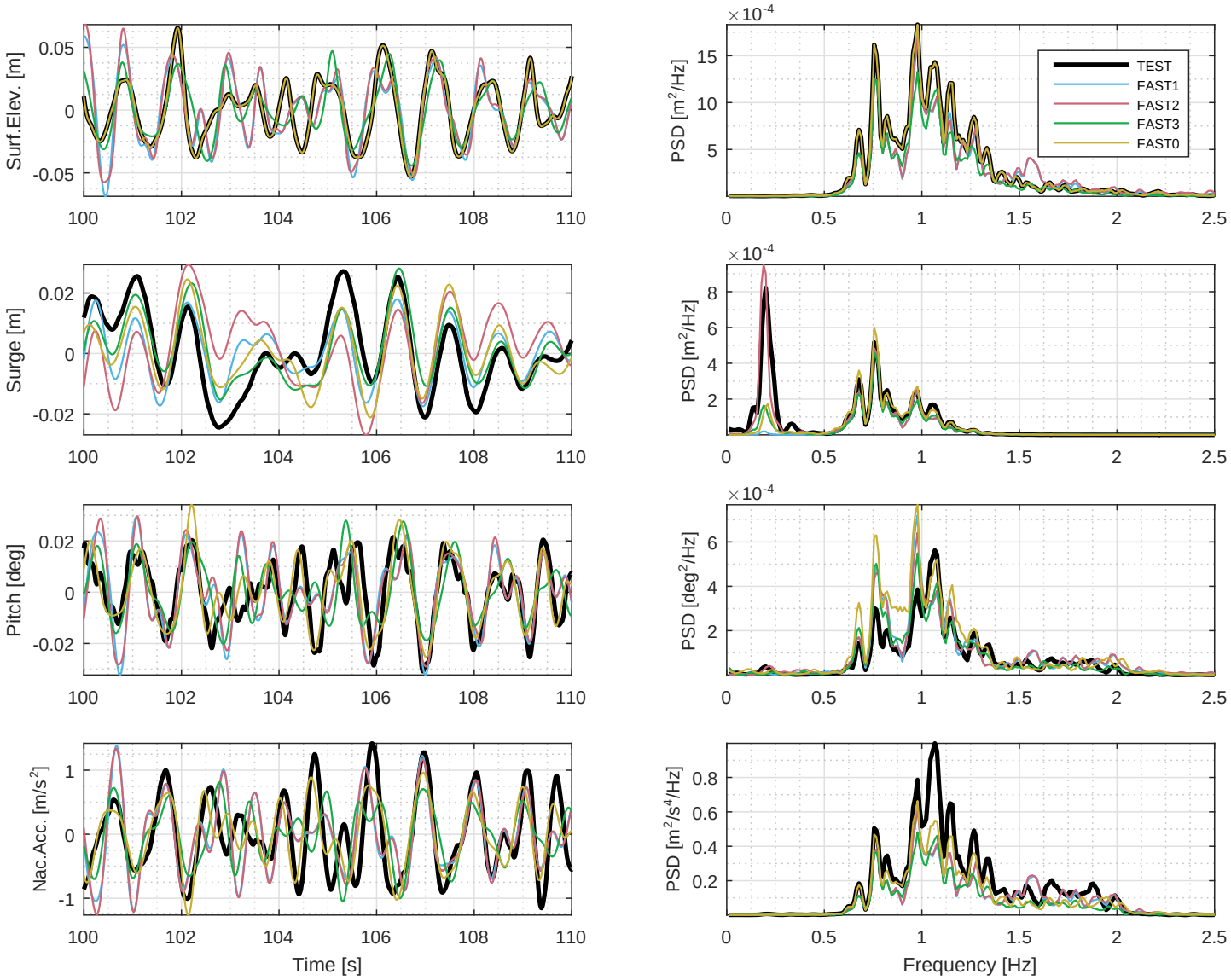

FIGURE 7. RESPONSE TO IRREGULAR WAVE I6-TIME SERIES AND PSD.

the absent sub and superharmonic excitation could be introduced if the first-order wave kinematics were extrapolated from the SWL up to the free surface. The extrapolation would introduce some second-order effects.

For the cases considered in this study and the methods applied, no particular choice of wave kinematics can be appointed as the "best choice" when it comes to accurate reproduction of test response at all frequencies and for all environmental conditions. The models with different sets of wave kinematics sometimes showed underprediction and some others overprediction of the test response. Therefore, a reasonable modeling approach would be to generate first-order wave kinematics from the measured signal when the corresponding test data are available and to employ nonlinear kinematics from the target signal otherwise—e.g., in a design scenario where test data do not exist.

One possible reason for the inconsistent behavior mentioned earlier could be the simplistic numerical damping employed in the model. The use of fully nonlinear wave kinematics only allows the user to introduce constant—independent of space and frequency—damping coefficients, which affect each degree of freedom globally. In the future, a more detailed, customizable definition of the user-defined numerical damping may help improve the affinity between numerical and experimental results.

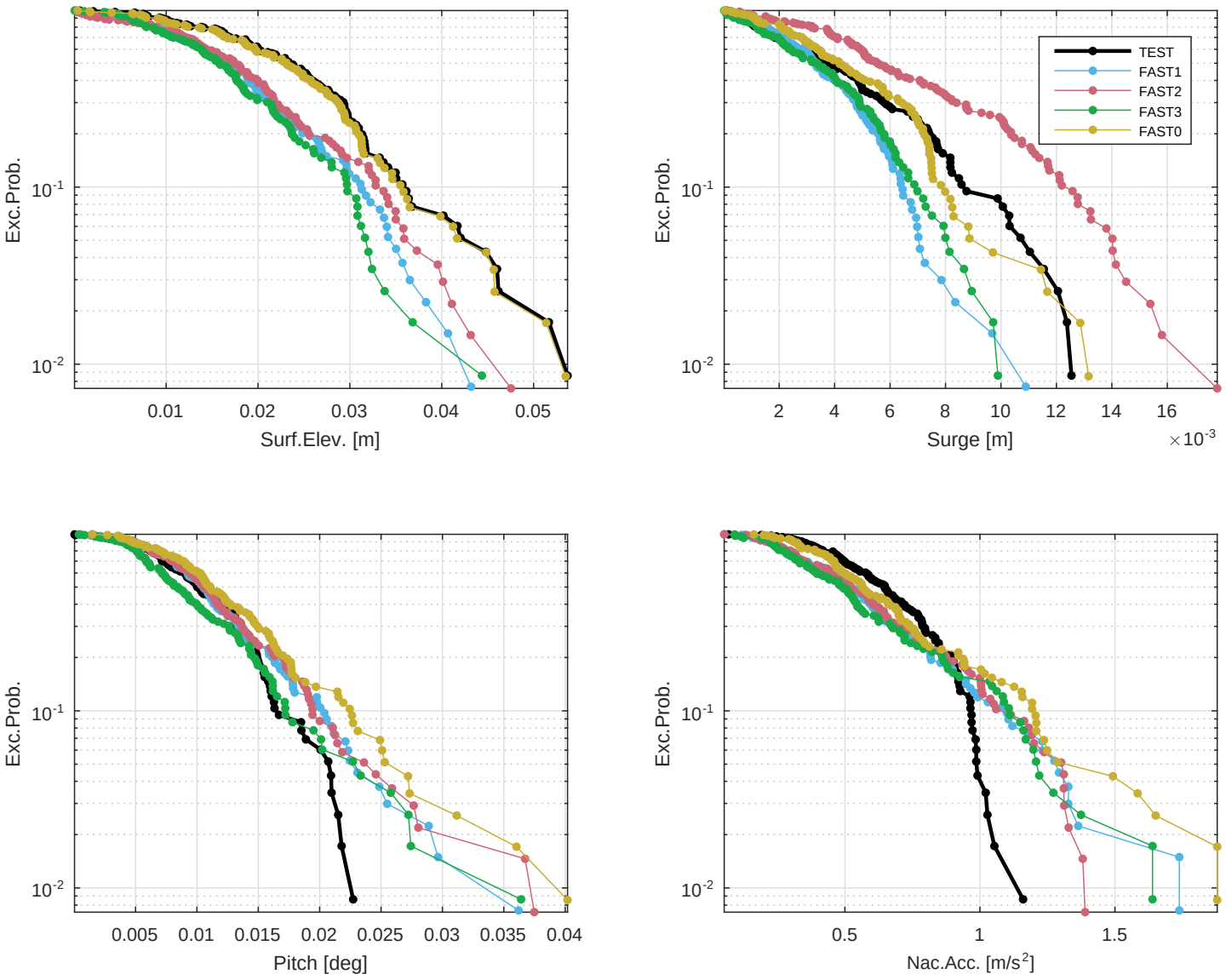

FIGURE 8. RESPONSE TO IRREGULAR WAVE I3-EXCEEDANCE PROBABILITY.

ACKNOWLEDGMENT

This work is part of the project LIFES50+ [19]. The research leading to these results has received funding from the European Union Horizon2020 programme under the agreement H2020-LCE-2014-1-640741. The experimental results were obtained as part of the INNWIND.EU project [30]. The NREL contribution was performed at NREL in support of the U.S. Department of Energy under Contract Number DE-AC36-08GO28308. The U.S. Government retains and the publisher, by accepting the article for publication, acknowledges that the U.S. Government retains a nonexclusive, paid-up, irrevocable, worldwide license to publish or reproduce the published form of this work, or allow others to do so, for U.S. Government purposes.

REFERENCES

[1] Airy, G., 1845. "Tides and waves". *Encycl. Metrop.*

[2] Morison, J., O'Brien, M., Johnson, J., and Schaaf, S., 1950. "The forces exerted by surface waves on monopiles". *J. Petrol. Techn.,* ***189***, pp. 149–154.

[3] Lee, C., and Newman, J., 2006. *WAMIT® User Manual, Versions 6.3, 6.3PC, 6.3S, 6.3S-PC*. Chestnut Hill, MA.

[4] Cummins, W., 1962. "The impulse response functions and

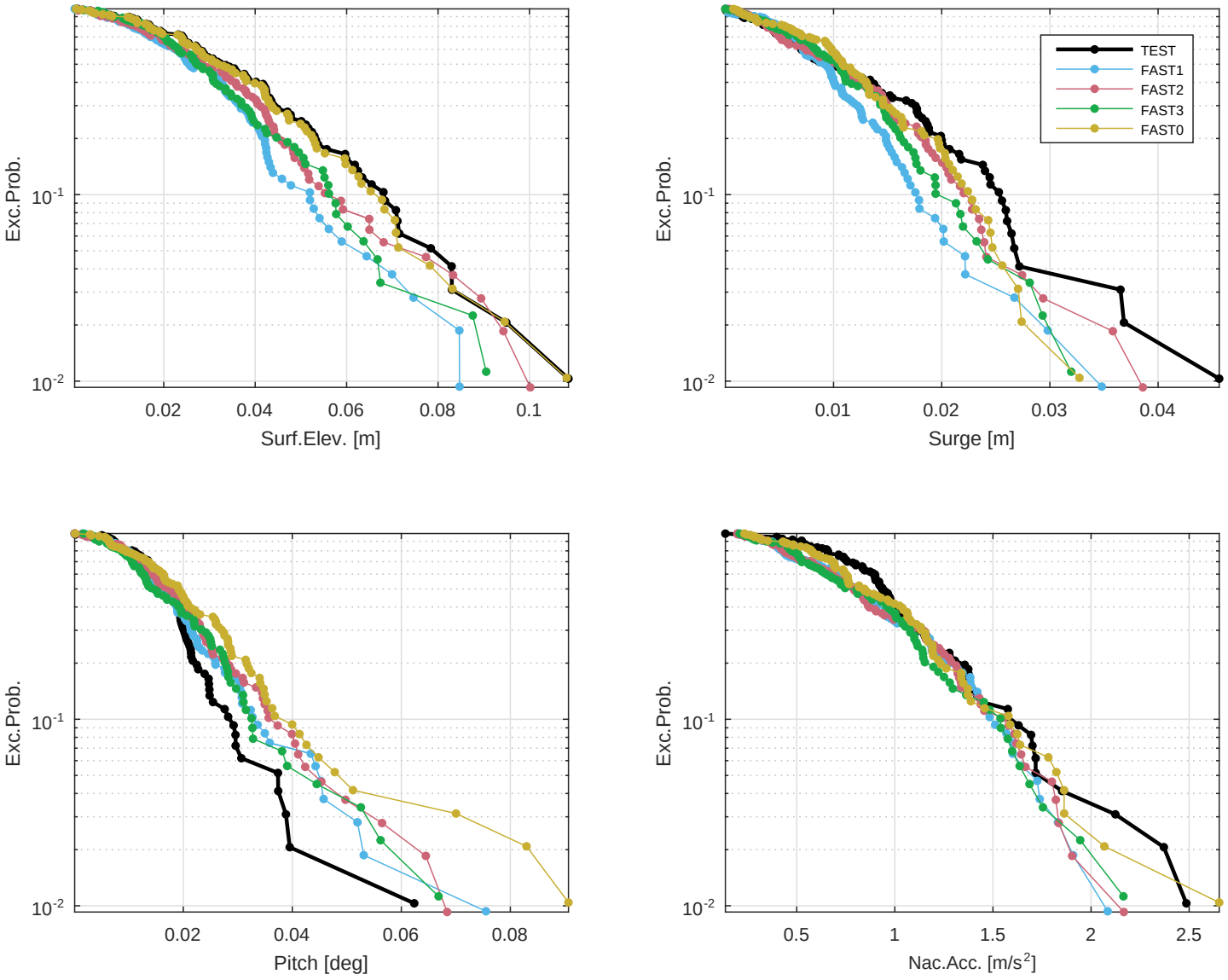

FIGURE 9. RESPONSE TO IRREGULAR WAVE I6-EXCEEDANCE PROBABILITY.

ship motions". *Schiffstechnik,* ***9***, pp. 101–109.

[5] Sharma, J., and Dean, R., 1981. "Second-order directional seas and associated wave forces". *Society of Petroleum Engineers Journal,* ***21***(01), pp. 129–140.

[6] Rainey, R., 1989. "A new equation for calculating wave loads on offshore structures". *Journal of Fluid Mechanics,* ***204***(1), pp. 295–324.

[7] Rainey, R., 1995. "Slender-body expressions for the wave load on offshore structures". *Proceedings of the Royal Society A: Mathematical, Physical and Engineering Sciences,* ***450***(1939), pp. 391–416.

[8] Sclavounos, P., 2012. "Nonlinear impulse of ocean waves on floating bodies". *Journal of Fluid Mechanics,* ***697***, pp. 316–335.

[9] Nematbakhsh, A., Bachynski, E., Gao, Z., and Moan, T., 2015. "Comparison of wave load effects on a TLP wind turbine by using computational fluid dynamics and potential flow theory approaches". *Applied Ocean Research,* ***53***, pp. 142–154.

[10] Øye, S., 1996. "FLEX4 simulation of wind turbine dynamics". In Proc. for the 28th IEA meeting of experts concerning state of the art of aero-elastic codes for wind turbine calculations.

[11] Jonkman, J., Butterfield, S., Musial, W., and Scott, G.,

2009. Definition of a 5-MW reference wind turbine for offshore system development. Tech. Rep. February, NREL.
[12] Schløer, S., Bredmose, H., Bingham, H., and Larsen, T., 2012. "Effects from fully nonlinear irregular wave forcing on the fatigue life of an offshore wind turbine and its monopile foundation". In Proceedings for the ASME 31st International Conference on Ocean, Offshore and Arctic Engineering (OMAE 2012).
[13] Schløer, S., 2013. "Fatigue and extreme wave loads on bottom fixed offshore wind turbines". PhD thesis, DTU.
[14] Schløer, S., Bredmose, H., and Bingham, H., 2016. "The influence of fully nonlinear wave forces on aero-hydro-elastic calculations of monopile wind turbines". *Marine Structures,* ***50***, pp. 162–188.
[15] Engsig-Karup, A., Bingham, H., and Lindberg, O., 2009. "An efficient flexible-order model for 3D nonlinear water waves". *Journal of Computational Physics,* ***228***(6), pp. 2100–2118.
[16] Bredmose, H., 2013. Contribution to INNWIND.EU deliverable 4.21: Nonlinear wave loads on a TLP floating wind turbine. Tech. rep., DTU Wind Energy.
[17] Dupont, M., and Aubrion, M., 2014. Nonlinear wave forcing on a floating wind turbine. MSc thesis, DTU.
[18] Pegalajar-Jurado, A., Bredmose, H., and Borg, M., 2016. "Multi-level hydrodynamic modelling of a scaled 10MW TLP wind turbine". *Energy Procedia,* ***94***, pp. 124–132.
[19] LIFES50+ project. http://lifes50plus.eu/.
[20] Jonkman, J., and Jonkman, B. NWTC Information Portal (FAST v8).
[21] Jonkman, J., 2009. "Dynamics of offshore floating wind turbines - Model development and verification". *Wind Energy,* ***12***(5), pp. 459–492.
[22] Chan, G., Sclavounos, P., Jonkman, J., and Hayman, G., 2015. "Computation of nonlinear hydrodynamic loads on floating wind turbines using fluid-impulse theory". In Proceedings for the ASME 34th International Conference on Ocean, Offshore and Arctic Engineering (OMAE 2015), Vol. 9.
[23] Roald, L., Jonkman, J., Robertson, A., and Chokani, N., 2013. "The effect of second-order hydrodynamics on floating offshore wind turbines". *Energy Procedia,* ***35***, pp. 253–264.
[24] Gueydon, S., Duarte, T., Jonkman, J., Bayati, I., and Sarmento, A., 2014. "Comparison of second-order loads on a semisubmersible floating wind turbine". In Proceedings for the ASME 33rd International Conference on Ocean, Offshore and Arctic Engineering (OMAE 2014).
[25] Gueydon, S., Wuillaume, P., Jonkman, J., Robertson, A., and Platt, A., 2015. "Comparison of second-order loads on a tension-leg platform for wind turbines". In Proceedings for the 25th International Offshore and Polar Engineering Conference (ISOPE 2015).
[26] Gueydon, S., and Jonkman, J., 2016. "Update on the comparison of second-order loads on a tension leg platform for wind turbines". In Proceedings for the 26th International Offshore and Polar Engineering Conference (ISOPE 2016).
[27] Bredmose, H., Mikkelsen, R., Hansen, A., Laugesen, R., Heilskov, N., Jensen, B., and Kirkegaard, J., 2015. Experimental study of the DTU 10 MW wind turbine on a TLP floater in waves and wind. Presented at EWEA Offshore 2015 Conference.
[28] Laugesen, R., and Hansen, A., 2015. Experimental study of the dynamic response of the DTU 10 MW wind turbine on a tension leg platform. MSc thesis, DTU.
[29] Pegalajar-Jurado, A., Hansen, A., Laugesen, R., Mikkelsen, R., Borg, M., Kim, T., Heilskov, N., and Bredmose, H., 2016. "Experimental and numerical study of a 10MW TLP wind turbine in waves and wind". *Journal of Physics: Conference Series,* ***753***.
[30] INNWIND.EU project. http://www.innwind.eu/.
[31] Tromans, P., Anaturk, A., and Hagemeijer, P., 1991. "A new model for the kinematics of large ocean waves - Application as a design wave". In Proceedings for the 1st International Offshore and Polar Engineering Conference (ISOPE 1991).
[32] Borg, M., Hansen, A., and Bredmose, H., 2016. "Floating substructure flexibility of large-volume 10MW offshore wind turbine platforms in dynamic calculations". *Journal of Physics: Conference Series,* ***753***.